

## Feasibility Study For Design And Utilization Of A Cold Neutron Irradiation Facility At The JSI TRIGA Reactor

**Diego Martín Cuéllar Fernández**

Faculty of Mathematics and Physics, University of Ljubljana  
Jadranska ulica 19  
1000, Ljubljana, Slovenia  
dc5899@student.uni-lj.si

**Gašper Žerovnik, Jan Malec**

Reactor Engineering Division, Jožef Stefan Institute  
Brinje 40  
1262, Dol pri Ljubljani, Slovenia  
gasper.zerovnik@ijs.si, jan.malec@ijs.si

### ABSTRACT

Typically, cold neutrons are considered to range from energies of 0.1 meV to 5 meV. Within this energy range, the cross sections for scattering and radiative capture are clearly outside the neutron resonance region. The need for increased accuracy in these cross section values arises from the discrepancies between different evaluated nuclear data libraries (ENDL) and experimental neutron cross section data. In this regard, a design of a cold neutron source using neutrons originating from the JSI TRIGA reactor core is proposed. A parametric study of this irradiation facility is performed using the computer code OpenMC for neutron transport calculations. Neutron beam is sampled and directed through a guide tube with a cold temperature moderator at the beginning, made of graphite or light-water (simulated as H<sub>2</sub> below 20K). At first, the simulation is done for a facility in the absence of targets, where cold neutron flux fractions are obtained and evaluated, using moderator thickness and temperature as degrees of freedom. It was found that for thicknesses of 90 cm in graphite and 20 cm in H<sub>2</sub>O the normalized cold neutron fluxes reached high values. Evaluation was made at different temperatures and the highest cold neutron fluxes were found at around 20 K and 58 K respectively for the moderators. With the combination of these moderator parameters, targets of <sup>207</sup>Pb and <sup>241</sup>Am were added and scattering and absorption reaction rates were obtained in the simulation, leading to the calculation of their respective cross sections over the cold energy range.

### 1 INTRODUCTION

With wavelengths comparable to interatomic distances and displaying resolved cross sections across its energy range (0.1 meV – 5 meV), cold neutrons are an important tool in research. In consequence, collective interference effects between atoms are important at these energy levels, hence, providing characteristic information about these bound atoms. Accurate cross section measurements are of vital importance for applications involving neutron reactions with matter and arose from the need to contrast discrepancies between different nuclear data libraries and experimental results.

Through cold neutron scattering, information on properties such as excited energy level states of nuclei, lifetimes of these states, excitation transitions, neutron tomography and crystal

structure can be performed [1]. On the other hand, cold neutron absorption is also useful for nuclear physics, reactor physics, reactor safety analyses, waste management and detector efficiency studies among other uses [2].

Given its benefits, cold neutron facilities, like the PGAA (Prompt Gamma-ray neutron Activation Analysis) at FRM II in Garching, Germany [3], open a possibility for studies at these neutron energy levels and were previously considered for the JSI TRIGA reactor before [4].

In this work, cold neutrons were used for a feasibility study of a cold neutron irradiation facility with the use of the open-source Monte Carlo code OpenMC [5], and the thermal and below-thermal scattering cross sections being processed with the computer software NJOY [6].

In this regard, a preliminary optimization study was envisioned to be performed by doing a moderator temperature/thickness parametric study in graphite and H<sub>2</sub>O/H<sub>2</sub> moderators. Thus, the cold neutron yields were obtained, and the absorption and scattering reaction rates and consequent macroscopic cross sections were followed in the cold neutron moderator. Selected targets of <sup>207</sup>Pb and <sup>241</sup>Am were also considered in the simulated facility, calculating their cross sections in the cold neutron energy range using the same Monte Carlo tool.

## 2 NUCLEAR DATA TREATMENT WITH NJOY

Evaluated nuclear data libraries, such as JEFF-3.3 [7], are reference nuclear data useful for the scientific community. Libraries are a distinctive tool for research in nuclear engineering and nuclear physics, including a diverse number of different data sets, from which the cross section data are of particular interest in the scope of this work.

However, at cold neutron energies, the collective effects of bound target nuclei are significant, where the fractional energy transfer between neutrons and nuclei is small. Since the wavelength of thermal or cold neutrons is larger than the range of the strong nuclear force (around 10<sup>-10</sup> m to 10<sup>-15</sup> m respectively), the incoming neutron does not have a good resolution of the target since its de Broglie wavelength is too large. Therefore, scattering comes entirely from the nucleus s-waves, showing a spherically symmetric-like behaviour [8]. Therefore, at these wavelengths, scattering is different and is defined as thermal scattering, nuclei must be treated collectively for both inelastic and elastic scattering.

From the expression of the neutron and scattered neutron wave functions, in a many bodies system, the expression of elastic scattering cross section is,

$$\left(\frac{d\sigma}{d\Omega}\right)_{\lambda\rightarrow\lambda'} = \frac{1}{\Phi} \sum_{k'} W_{k,\lambda\rightarrow k',\lambda'}, \quad (1)$$

where  $\lambda$  and  $\lambda'$  are the initial and final state of the scattering system respectively,  $\mathbf{k}$  and  $\mathbf{k}'$  the incident and the final neutron wavevectors respectively and  $W_{k,\lambda\rightarrow k',\lambda'}$  describes the number of transitions per second from initial to final state. By applying Fermi's golden rule to calculate the rate of the state transitions,

$$\sum_{k'} W_{k,\lambda\rightarrow k',\lambda'} = \frac{2\pi}{\hbar} \rho_{k'} |\langle \mathbf{k}'\lambda' | V | \mathbf{k}\lambda \rangle|^2, \quad (2)$$

$\rho_{k'}$  is the density of momentum states in  $d\Omega$  per unit energy for  $\mathbf{k}'$  neutrons,  $\hbar$  the reduced Planck constant. The notation  $|\langle \mathbf{k}'\lambda' | V | \mathbf{k}\lambda \rangle|$  represents the matrix element describing the transition from initial to final state through the interaction potential  $V$ .

$$\left(\frac{d^2\sigma}{d\Omega dE'}\right)_{\lambda\rightarrow\lambda'} = \frac{k'}{k} \left(\frac{m}{2\pi\hbar^2}\right)^2 |\langle \mathbf{k}'\lambda' | V | \mathbf{k}\lambda \rangle| \delta(E_\lambda - E_{\lambda'} + E - E'). \quad (3)$$

where  $\delta$  is the Dirac distribution for the energy conservation between pre and post scattering states of both system (subscript  $\lambda$ ) and neutron.

For inelastic scattering at thermal energies, the energy transfer is made to the phonon distribution of the nuclei of the scattering system. To simplify matters, the incoherent approximation is used for crystalline moderator solids, stating that interference effects between nuclei are comparatively small, therefore coherent inelastic scattering is negligible. The scattering “law” defines inelastic scattering in consequence:

$$S(\alpha, \beta) \equiv \frac{1}{2\pi} \int_{-\infty}^{\infty} \int e^{i(\alpha r - \frac{\beta t}{\hbar})} G(\mathbf{r}, t) d\mathbf{r} dt. \quad (4)$$

The scattering “law”  $S(\alpha, \beta)$  is used to describe the phonon energy transfer in function of two main unitless variables  $\alpha$  and  $\beta$  representing the momentum and energy change respectively.  $G(\mathbf{r}, t)$  is the ‘pair distribution function’ at position  $\mathbf{r}$  and time  $t$ . In the absence of quantum effects,  $G$  can be interpreted as the probability of encountering a second atom inside an infinitesimal unit volume [9].  $\alpha$  and  $\beta$  are given by:

$$\alpha = \frac{E' + E - 2\mu\sqrt{E'E}}{A k_b T}, \quad (5)$$

$$\beta = \frac{E' - E}{k_b T}, \quad (6)$$

where  $\mu$  is the cosine of the scattering angle,  $E$  and  $E'$  the energies before and after collision.  $k_b$  the Boltzmann constant,  $T$  the neutron temperature and  $A$  the mass ratio between scatterer nucleus and neutron.

Following these equations, the code NJOY [6], by the use of its modules LEAPR and THERMR, respectively calculates the scattering law  $S(\alpha, \beta)$  and calculates pointwise cross sections for thermal and below energy ranges both graphite [10] and H<sub>2</sub>O/ H<sub>2</sub> [11].

### 3 FACILITY DESIGN AND NEUTRON TRANSPORT SIMULATION IN OPENMC

Once the thermal scattering cross section data generated with the help of NJOY for eight linearly spaced temperatures in the cold range (from 5 K to 57.94 K) and, for comparison, two in the thermal range (174.56 K and the standard temperature 293.15 K).

Following the technical specifications shown by the descriptions of the PGAA facility in Garching, Germany [3]; as well as the NIST reactor cold source facility [12], the cold source of the irradiation channel is designed, with a length of 200 cm along the x-axis and a square with 2.5 cm sides along the y and z-axes, as described in Figure 1. Periodic boundaries were set to avoid the loss of neutrons through the walls. The moderator region was placed in the middle of the channel with variable thickness, following different thickness sets, differing for the different types of moderators, which were determined by preliminary simulations of the cold neutron facility. The entrance and exit boundaries, as well as the ones corresponding to the moderator region were set as transmissive.

The transit medium is composed of a laboratory grade vacuum at 1 mbar pressure with air density of  $1.19 \cdot 10^{-6}$  g/cm<sup>3</sup>. The moderator is either composed of graphite with <sup>12</sup>C/<sup>13</sup>C isotopic ratio of around 99:1 or typical pure H<sub>2</sub>O/H<sub>2</sub>, the latter having a density of around 0.07 g/cm<sup>3</sup> at 20 K. Targets were also defined to study the behaviour of, first, a stable nucleus defined by the nuclear reaction <sup>207</sup>Pb(n,  $\gamma$ )<sup>208</sup>Pb [13] and of in a highly absorbing nucleus corresponding to the nuclear reaction <sup>241</sup>Am(n,  $\gamma$ )<sup>242</sup>Am [14]. Pure material targets were simulated as a small cylinder of 1 cm radius and 0.5 cm height bound to a 0.1 cm thick square holder of pure <sup>27</sup>Al.

The source was defined to follow a typical TRIGA central channel spectrum. Data of the spectrum was provided by JSI and implemented in the OpenMC code.

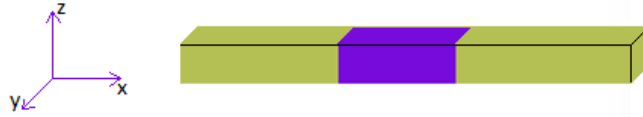


Figure 1: Scheme of the OpenMC representation of the cold neutron simulated facility. The golden area represents the transit medium, while the purple area represents the moderator region.

## 4 MONTE CARLO SIMULATION OF THE COLD NEUTRON FACILITY

Using the setup described previously, OpenMC was run for the cases of a graphite and light-water/liquid-hydrogen cold neutron moderator, afterwards adding  $^{207}\text{Pb}$  and  $^{241}\text{Am}$  targets. In the former, the normalized cold neutron fractions were obtained at the end of the channel, and for the targets the macroscopic cross sections were obtained using the following expression:

$$\Sigma = \sigma N_d = R/\phi. \quad (7)$$

where  $\Sigma$  is the macroscopic cross section in  $\text{cm}^{-1}$ ,  $\sigma$  is the microscopic cross section (barn or  $\text{cm}^2$ ),  $N_d$  the atomic density in  $\text{cm}^{-3}$ ,  $R$  is the reaction rate in  $\text{cm}^{-3} \text{s}^{-1}$ , and  $\phi$  is the unidirectional and invariant speed neutron beam flux in  $\text{cm}^{-2} \text{s}^{-1}$ . By the use of tallies defined by spatial, energetic and geometric restrictions, OpenMC obtains  $R$  for every region of the facility and calculates  $\Sigma$ .

### 4.1 Graphite moderator

In a first time, graphite was used in the designed facility. The cold neutron flux was obtained for the simulation at various moderator thicknesses  $t_{mod}$ , up to 150 cm and for different temperatures, described previously in section 3.

Cold neutron fractions increase following sigmoid tendencies with  $t_{mod}$  for all considered temperatures, depicted in Figure 2, with almost no increase below  $t_{mod} = 10$  cm, and then sharply increase until around  $t_{mod} \sim 80\text{-}90$  cm, reaching a saturated region henceforth.

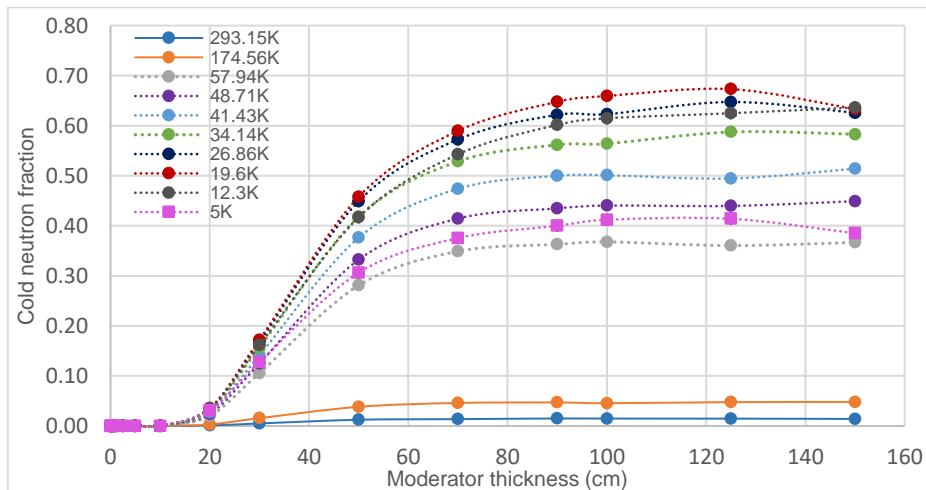


Figure 2: Cold neutron fraction as a function of graphite moderator thickness at different graphite temperatures. The statistical uncertainties are relatively low and thus, unnoticeable, except for lower temperatures and  $t_{mod} \geq 130$  cm.

Cold neutron fractions are found to be higher in the cold neutron range ( $< 57.94$  K) than in the thermal range ( $> 57.94$  K) as expected. There is an increase in the cold neutron fraction at all thicknesses at around  $\sim 19.6$  K, where the cold neutron fractions reach maximum values, with subsequent sharp decrease at lower temperatures, as evidenced for 12.3 K and 5 K. This effect can be attributed to the increase of the absorption cross section for lower energy cold neutrons.

In fact, the increase in absorption cross section is exacerbated as the temperature drops further, increasing considerably at 5 K. Although scattering cross sections are comparably much higher than absorption (about two orders of magnitude), scattering decreases along with temperature. This combined effects, seen in Figure 3 cause the presence of an optimal cold neutron yield for temperatures around 19.6 K. In most cases the optimal neutron fractions are obtained at around 90 cm. As temperature drops further, high absorption causes the cold neutron flux to diminish considerably, producing a drop in the relative availability of cold neutrons.

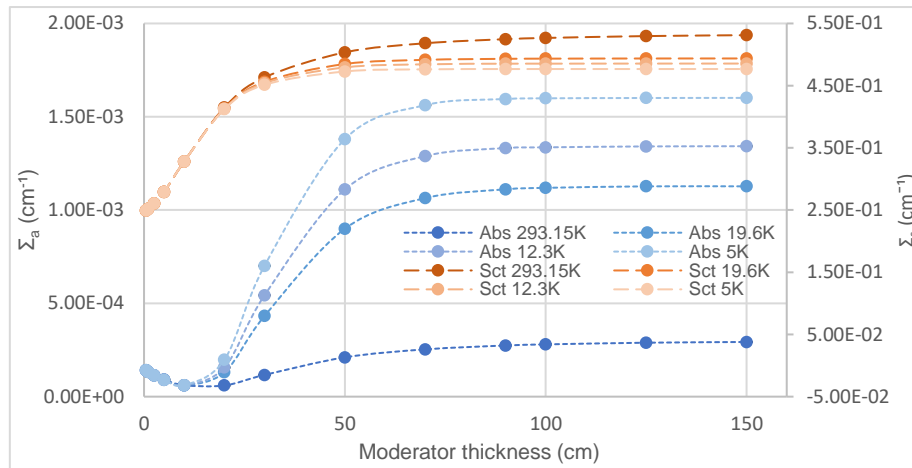


Figure 3: Absorption,  $\Sigma_a$ , and scattering,  $\Sigma_s$ , macroscopic cross sections inside graphite moderator region as a function of thickness for different selected representative temperatures of 5 K, 12.3 K, 57.94 K and 293.15 K. The statistical uncertainties are relatively low and thus, unnoticeable here.

## 4.2 Light-water/liquid-hydrogen moderator

Cold neutron fractions were also obtained for different moderator temperatures, defined in section 3, and thicknesses ranging up to 50 cm, as depicted in Figure 4.

The needed thickness is lower than in graphite. No divergence is shown at  $t_{mod} < 1$  cm for all temperatures. After this threshold, a rapid exponential-like growth phase for  $H_2O$  is evidenced, milder for  $H_2$ , with its steepness increasing nonlinearly with temperature drop. Then, a region of slower increase is observed for  $t_{mod} \geq 10$  cm, but this time a drop in the cold neutron fraction occurs at  $t_{mod} > 20$  cm for all temperatures for  $H_2O$  except for the standard temperature where the drop starts at above 40 cm, and below 20 K when  $H_2$  is used. The cold neutron fraction reaches maxima for most temperatures at around 20 cm. At  $t_{mod} > 1$  cm, the cold neutron fraction is shown to increase as temperatures drops down to 57.94 K. For lower temperatures, cold neutron fractions begin to decrease. The optimal cold neutron fraction is thus found for a temperature of 57.94 K.

Cold absorption in light-water is found to be constantly increasing with temperature drop of the moderator. However, for  $H_2$ , a decrease in the observed absorption is evidenced. As moderator thickness increases, a rapid exponential-like increase phase spans until  $t_{mod} \sim 20$  cm for  $H_2O$  and a bit further for  $H_2$  ( $t_{mod} \sim 25$  cm). Then a threshold is reached and values for moderator  $\Sigma_a$  seem to reach an asymptote. This behavior is witnessed for every considered temperature in the thermal and cold energy ranges indiscriminately.

On the other hand, scattering is more important for higher temperatures while decreasing along the temperature. The gap between each  $\Sigma_s$  temperature lines close as the temperature decreases further, having narrower temperature lines and meaning a reduction of temperature sensitivity at lower cold region temperatures. This effect opposes the one found for  $\Sigma_a$  in light-water, where temperature drop increases the moderator absorption. Although the variance decreases at the lower temperature limit of the cold region, both scattering and absorption reach an asymptote at around  $t_{mod} = 20$ -25 cm, point where  $\Sigma_s/\Sigma_a$  tends to its minimum, explaining

the decrease of the cold neutron fraction, as seen in Figure 5. At around  $t_{mod} = 10$  cm, absorption tends to become predominant with respect to absorption for temperatures below 58 K. At cold temperatures, absorption and scattering do not vary much when considering liquid-hydrogen.

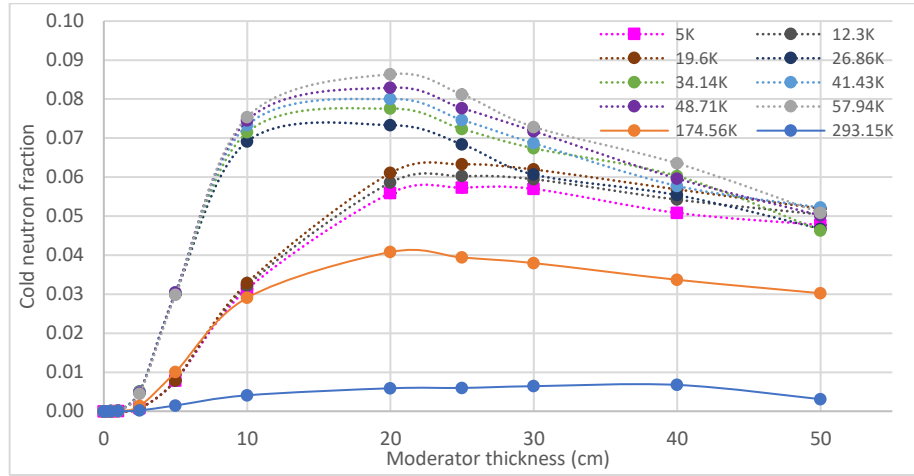


Figure 4: Cold neutron fraction as a function of H<sub>2</sub>O/H<sub>2</sub> moderator thickness for different temperatures. No error bars are shown since the statistical uncertainties are considerably low.

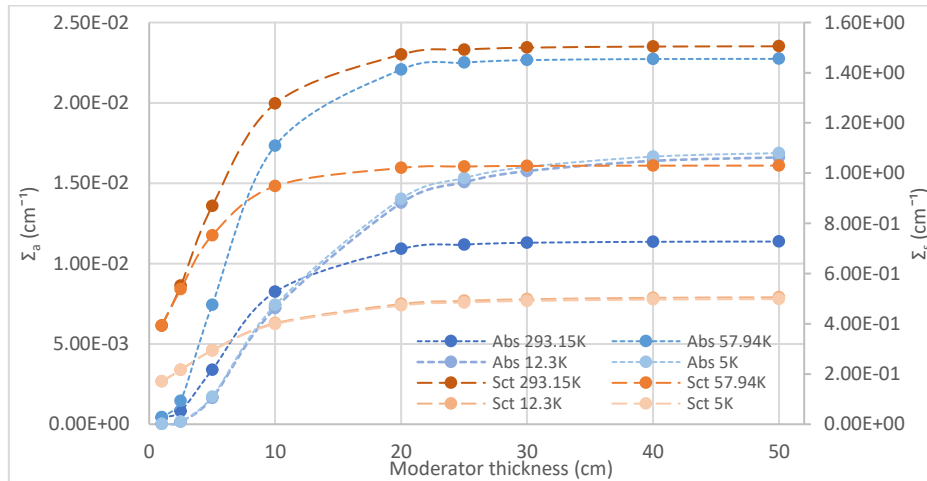


Figure 5: Absorption,  $\Sigma_a$ , and scattering,  $\Sigma_s$ , macroscopic cross sections for light-water/liquid-hydrogen moderator as a function of thickness for different selected representative temperatures of 5 K, 12.3 K, 57.94 K and 293.15 K. The statistical uncertainties are relatively low and thus, unnoticeable.

### 4.3 Cross section determination in <sup>207</sup>Pb and <sup>241</sup>Am with OpenMC

Targets of <sup>207</sup>Pb and <sup>241</sup>Am are simulated in the cold neutron facility, as described in section 3. Using eq.7, the energy dependent microscopic cross sections can be determined and are normalized in eq.8 with the help of a normalization factor,  $\sigma_n \sqrt{E_n/E}$ , using the cross section  $\sigma_n$  corresponding to the thermal standard energy (293.15 K),  $E_n$ , obtained using JANIS nuclear data plotting tool [15].

$$\sigma(E)/\sigma_n \sqrt{E/E_n} . \quad (8)$$

The normalized cross sections for both nuclides are found to be independent respecting to the moderator temperature and are plotted in Figure 6. After normalization, as expected, the absorption cross sections were constant along the cold neutron energy range and thus, do follow a  $1/v$  relation. On the other hand, the scattering cross section showed a decreasing tendency for both targets and do not follow the  $1/v$  "law". This trend is similar for each target.

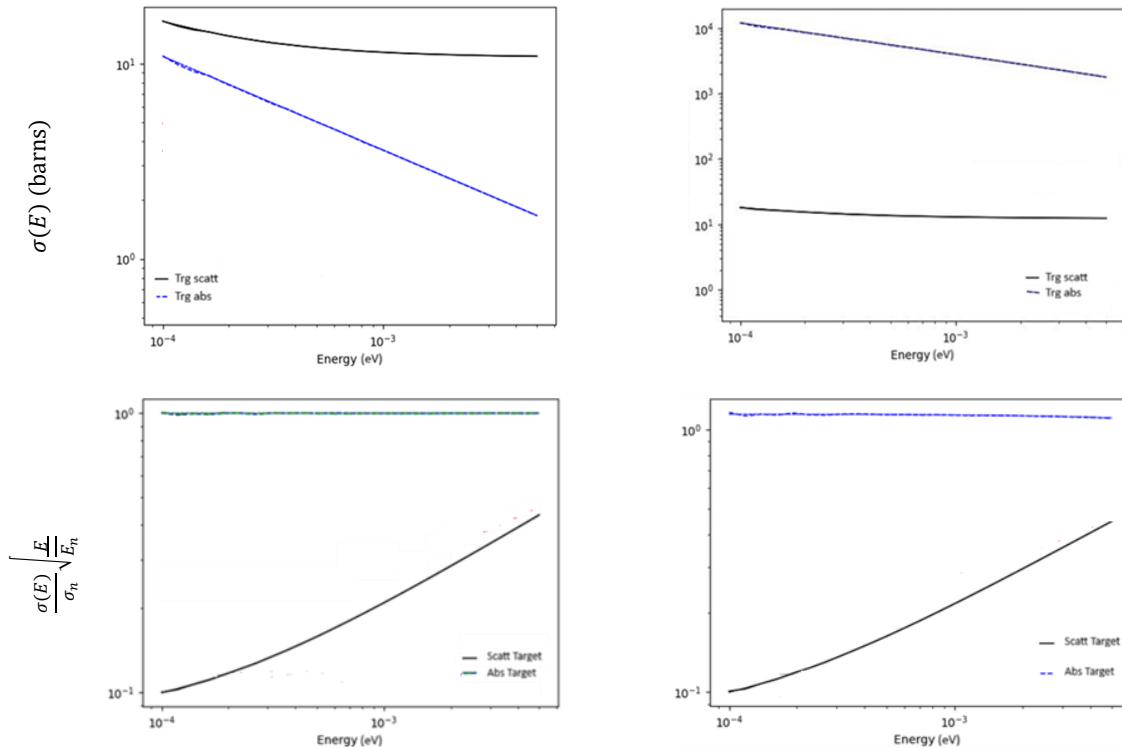


Figure 6: Simulated (up) and normalized (down) microscopic cross sections for  $^{207}\text{Pb}$  (left) and  $^{241}\text{Am}$  (right) in the cold neutron energy region.

## 5 CONCLUSIONS

With the proposed geometry and materials after thermal scattering treatment via the scattering “law”, a simulation of the proposed cold neutron facility was performed, and a parametric analysis of moderator thickness and moderator temperature was carried out for graphite and light-water with a liquid-hydrogen correction model for temperatures below 20 K. Normalized cold neutron fractions, absorption and scattering macroscopic cross sections for both cases were evaluated using OpenMC.

$\Sigma_a$  increased for graphite and  $\text{H}_2\text{O}$  while moderator temperature decreased and thickness increased. For  $\text{H}_2$ , a decrease respecting to  $\text{H}_2\text{O}$  was noticed. Neighbouring temperature line gaps increased at lower temperatures in graphite, while they decreased in the other case. Big differences were found between absorption values in the thermal and cold region for  $\text{H}_2\text{O}$ , but not for  $\text{H}_2$ .  $\Sigma_a$  in light-water was at least one order of magnitude greater than in graphite.

Scattering revealed also differences between both moderators. At thermal temperatures,  $\Sigma_s$  in  $\text{H}_2\text{O}/\text{H}_2$  was one order of magnitude greater than in graphite, with a decrease of the difference for cold temperatures. It was noted that scattering in graphite does not decrease very much with temperature, whereas for  $\text{H}_2\text{O}/\text{H}_2$ , the scattering is much more important for thermal temperatures (up to two times). The increase of thickness caused increased scattering as expected.

A higher cold neutron flux was found after neutrons travelled through graphite respecting to light-water/liquid-hydrogen. Competitiveness of absorption and scattering dictated the outcome of the overall cold neutron yield and the differences between considered moderators, favouring the yields in graphite since  $\Sigma_a$  is much more important in  $\text{H}_2\text{O}/\text{H}_2$ . For  $t_{mod} \sim 90$  cm in graphite and a moderator temperature of 19.6 K, cold neutron fraction reached a value of around 65%. Meanwhile, in  $\text{H}_2\text{O}/\text{H}_2$ , for 20 cm and at 57.94 K, maximum cold neutron fraction reached 8.64%. This difference favours the use of graphite as cold neutron moderator, although deeper analyses must be performed to determine true optimal thickness and temperature in both cases.

Finally, the simulated cold neutron facility was used for neutron irradiation of  $^{207}\text{Pb}$  and  $^{241}\text{Am}$  targets, and microscopic cross sections were calculated and found to be in accordance with cross section data from JEFF-3.3. Normalization showed a  $1/v$  dependence for absorption cross sections but not for scattering, as expected. Furthermore, no moderator temperature variability was evidenced. This preliminary study shows that a cold neutron irradiation channel is feasible from the theoretical point of view, and relatively high cold neutron fluxes could be produced using the TRIGA reactor to perform different cross section measurements for nuclear reactions with the adequate equipment and setup and use improved versions of this code as benchmarks.

## ACKNOWLEDGMENTS

This work was done with the support of Jožef Stefan Institute and University of Ljubljana.

## REFERENCES

- [1] M. L. Martins, W. P. Gates, L. Michot, E. Ferrage, V. Marry and H. N. Bordallo, "Neutron scattering, a powerful tool to study clay minerals", *Applied Clay Science*, 96, 2014, pp. 22-35.
- [2] T. Kitagaki, K. Sakai, M. Hino, M. Utsuro, M. Higuchi, P. Geltenbort and J. Butterworth, "An abnormal ultra-cold-neutron absorption in solid UCN-detectors", *Nuclear Instruments and Methods in Physics Research Section A: Accelerators, Spectrometers, Detectors and Associated Equipment*, 529, 2004, pp. 425-428.
- [3] P. Kudejova, G. Meierhofer, K. Zeitelhack, J. Jolie, R. Schulze, A. Türler and T. Materna, "The new PGAA and PGAI facility at the research reactor FRM II in Garching near Munich", *J. Radioanal. Nucl. Chem.*, 278, 2008, pp. 691-695.
- [4] V. Dimic and J. Petkovsek, "Construction and performance of the liquid methane cold source", *J. Phys. E: Sci. Instrum.*, 4, 1971, pp. 905.
- [5] P. K. Romano and B. Forget, "The OpenMC Monte Carlo Particle Transport", *Annals of Nuclear Energy*, 51, 2013, pp. 274–281.
- [6] R. Macfarlane, D. W. Muir, R. M. Boicourt, A. C. Kahler, J. L. Conlin and W. Haeck, "The NJOY Nuclear Data Processing System, Version 2016", LA-UR--17-20093, Los Alamos National Laboratory, Jan 2017.
- [7] A. Plompen, O. Cabellos, C. De Saint Jean et al., "The joint evaluated fission and fusion nuclear data library, JEFF-3.3", *Eur. Phys. J. A*, 56, 2020, pp. 181.
- [8] G. Squires, *Thermal Neutron Scattering*, Cambridge University Press, 1978, pp. 10-24.
- [9] G. Bell and S. Glasstone, *Nuclear Reactor Theory*, Van Nostrand Reinhold, 1970, pp. 315-341.
- [10] M. Mattes and J. Keinert, "Status of Thermal Neutron Scattering Data for Graphite", INDC(NDS)--0475, International Atomic Energy Agency, 2005.
- [11] R. E. MacFarlane, "New Thermal Neutron Scattering Files for ENDF/B-VI Release 2", LA--12639-MS, Los Alamos National Laboratory, 1994.
- [12] H. J. Prask, J. M. Rowe, J. J. Rush and I. G. Schröder, "The NIST Cold Neutron Research Facility". *J. Res. Natl. Inst. Stand. Technol.*, 98, 1993, pp. 1-13.
- [13] T. Belgya, B. Fazekas, Z. Kasztovszky, Z. Révay, G. Molnár, M. Yeh, P. E. Garrett and S. W. Yates, "Levels of  $^{208}\text{Pb}$  from the  $^{207}\text{Pb}(n,\gamma)$  reaction with a guided neutron beam", *Phys. Rev. C*, 57, 1998, 2740-2743.
- [14] C. Genreith, M. Rossbach, Z. Révay and P. Kudejova, "Determination of  $(n,\gamma)$  Cross Sections of  $^{241}\text{Am}$  by Cold Neutron Activation", *Nuclear Data Sheets*, 119, 2014, pp. 69-71.
- [15] N. Soppera, M. Bossant and E. Dupont, "JANIS 4: An Improved Version of the NEA Java-based Nuclear Data Information System", *Nuclear Data Sheets*, 120, 2014, pp. 294-296.